THE JOURNAL OF PHYSICAL CHEMISTRY B
A JOURNAL OF THE AMERICAN CHEMICAL SOCIETY

pubs.acs.org/JPCB

Article

An Exciton Dynamics Model of *Bryopsis corticulans* Light-Harvesting Complex II

Published as part of The Journal of Physical Chemistry virtual special issue "Yoshitaka Tanimura Festschrift".

Hoang Long Nguyen, Thanh Nhut Do, Parveen Akhtar, Thomas L.C. Jansen, Jasper Knoester, Wenda Wang, Jian-Ren Shen, Petar H. Lambrev,* and Howe-Siang Tan*

Cite This: *J. Phys. Chem. B* 2021, 125, 1134–1143

Read Online

ACCESS | Metrics & More | Article Recommendations | Supporting Information

ABSTRACT: *Bryopsis corticulans* is a marine green macroalga adapted to the intertidal environment. It possesses siphonaxanthin-binding light-harvesting complexes of photosystem II (LHCII) with spectroscopic properties markedly different from the LHCII in plants. By applying a phenomenological fitting procedure to the two-dimensional electronic spectra of the LHCII from *B. corticulans* measured at 77 K, we can extract information about the excitonic states and energy-transfer processes. The fitting method results in well-converged parameters, including excitonic energy levels with their respective transition dipole moments, spectral widths, energy-transfer rates, and coupling properties. The 2D spectra simulated from the fitted parameters concur very well with the experimental data, showing the robustness of the fitting method. An excitonic energy-transfer scheme can be constructed from the fitting parameters. It shows the rapid energy transfer from chlorophylls (Chls) *b* to *a* at subpicosecond time scales and a long-lived state in the Chl *b* region at around 659 nm. Three weakly connected terminal states are resolved at 671, 675, and 677 nm. The lowest state is higher in energy than that in plant LHCII, which is probably because of the fewer number of Chls *a* in a *B. corticulans* LHCII monomer. Modeling based on existing Hamiltonians for the plant LHCII structure with two Chls *a* switched to Chls *b* suggests several possible Chl *a*−*b* replacements in comparison with those of plant LHCII. The adaptive changes result in a slower energy equilibration in the complex, revealed by the longer relaxation times of several exciton states compared to those of plant LHCII. The strength of our phenomenological fitting method for obtaining excitonic energy levels and energy-transfer network is put to the test in systems such as *B. corticulans* LHCII, where prior knowledge on exact assignment and spatial locations of pigments are lacking.

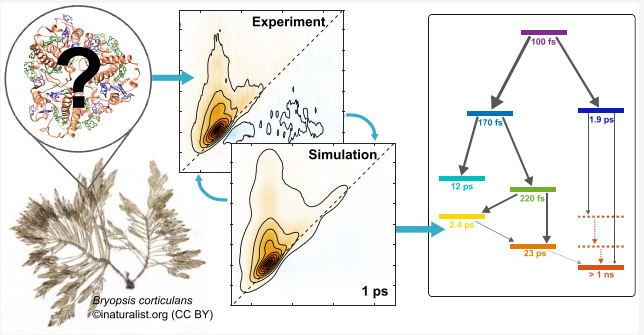

1. INTRODUCTION

Photosynthesis is a process employed by plants and other organisms, such as green algae and cyanobacteria, where they absorb sunlight and convert it into biochemical energy to power life on Earth.[1] Light-harvesting complex II (LHCII) is a light-harvesting antenna associated with photosystem II (PSII) that is responsible for the absorption of light in photosynthesis. The harvested light is transferred between the pigments in the complex, then funneled to the other complexes in the PSII and eventually to a photosynthetic reaction center where it is used to drive photochemical reactions.[1] The mechanism of the ultrafast and efficient excitation energy-transfer (EET) processes happening in LHCII still remains to be fully elucidated.[2]

Bryopsis corticulans (*B. corticulans*) is a species of siphonous marine green macroalgae that can be found at intertidal shores. The alga has adapted its LHCII structure to the fast fluctuation of light and dominance of blue-green light in its living environment.[3] LHCII in *B. corticulans* exists in the trimeric form with each monomeric unit containing 14 chlorophylls (Chls), which is similar to higher-plant LHCII.[4] However, in contrast to the LHCII of higher plants where these 14 Chls comprise of eight Chl *a* and six Chl *b* molecules,[5,6] it has been shown from spectroscopic and pigment analyses that the opposite ratio (eight Chl *b* and six Chl *a* molecules) holds for the LHCII in *B. corticulans*.[4] Chl *b* molecules absorb light at higher frequencies than Chl *a* molecules in the Q_y region, so this Chl composition variation helps *B. corticulans* adapt to the underwater environment where less red light is available and

Received: November 26, 2020
Revised: January 14, 2021
Published: January 22, 2021

Table 1. Mean Values and Standard Deviations of the Excitonic Levels, Transition Dipole Moments, Spectral Widths, and Anti-Diagonal Widths (Half-Width at Half-Maximum)[a,b]

Excitonic level		Relative transition dipole moment (a.u.)	Spectral width (cm^{-1})	Anti-diagonal width (cm^{-1})
Wavelength (nm)	Wavenumber (cm^{-1})			
650	15391.6 ± 0.4	1.000	100.0 ± 0.0*	99.6 ± 2.3
659	15179 ± 2	0.790 ± 0.008	98.5 ± 1.4	50 ± 11
659′	15176 ± 2	0.772 ± 0.006	95.3 ± 1.3	79 ± 11
667	14999.4 ± 0.1	0.735 ± 0.001	68.7 ± 0.1	58.9 ± 0.4
668	14969.6 ± 0.4	0.774 ± 0.001	75.6 ± 0.2	75.6 ± 0.2
671	14897.3 ± 0.1	0.750 ± 0.002	54.2 ± 0.1	29.5 ± 0.0*
675	14817.3 ± 0.1	0.898 ± 0.001	49.2 ± 0.0*	24.3 ± 0.0*
677	14761.8 ± 0.2	0.749 ± 0.000#	73.9 ± 0.0*	41.0 ± 0.2

[a]The results were averaged among the best 80 fits. The wavelengths were derived from the mean wavenumbers. The first dipole moment is fixed at 1, so there is no standard deviation. The green shading indicates the high-energy region (λ < 660 nm), where the states are probably from Chls *b*. The red shading indicates the low-energy region (λ > 660 nm), where the states are probably from Chls *a*. [b]The asterisk (*) represents that the standard deviation is less than 0.05, and the pound sign (#) represents that the standard deviation is less than 0.0005.

blue-green light is more dominant.[3] The adaptation may affect the photosynthesis activities of the organism; thus, studying the effects on the EET processes may lead to new understandings about photosynthesis.

The structure of *B. corticulans* LHCII has not yet been reported, although the overall structure is expected to resemble the closely related higher-plant LHCII.[4] Presently, therefore, this precludes the theoretical structure-based modeling of detailed EET dynamics and probably explains why there have been only a few studies reporting on the EET in LHCII from *B. corticulans*.[7,8] The EET from LHCII of a related species, *Bryopsis maxima*, was studied a few decades ago by Nakayama et al. using picosecond fluorescence spectroscopy at both physiological and cryogenic temperatures.[9] Several EET time scales from carotenoids and Chls *b* to Chls *a* were observed at 77 K, with the fastest resolved energy flow on a time scale of ~20 ps from 672 to 679 nm Chl *a* states. This observation is similar to the last step of the energy equilibration in higher-plant LHCII at 77 K that was reported in previous studies by several of us.[10,11] Only recently, LHCII from *B. corticulans* was studied and shown to exhibit a longer fluorescence lifetime and a higher fluorescence quantum yield than higher-plant LHCII.[12,13] The ultrafast dynamics in *B. corticulans* LHCII have also been recently investigated using time-resolved fluorescence spectroscopy and two-dimensional electronic spectroscopy (2DES).[12] Population transfers between Chls were observed at various time scales from hundreds of femtoseconds to several picoseconds. Distinct features, such as the presence of long-lived Chls *b* and the slow equilibration in the Chl *a* pools, were also pointed out. However, these studies did not provide a detailed picture about the EET process, which in theory can be derived from 2D spectra as has been shown theoretically[14] and implemented experimentally.[11,15]

In this work, we present a model for the EET in LHCII from *B. corticulans* at 77 K, which was obtained by performing a fitting procedure using a phenomenological description.[14] This phenomenological approach has been previously applied to resolve the EET networks in the Fenna−Matthews−Olson complex of green sulfur bacteria[15] and recently, with suitable modifications, the energy-transfer network in plant LHCII.[11] The advantage of this phenomenological approach is that it can extract information about the excitonic energy levels and population dynamics at the level of microscopic transfer rates of a system solely from the 2DES data. Thus, this technique is most useful to study systems such as *B. corticulans* LHCII, where prior knowledge and structure-based calculations are lacking. Although the 2D spectra of LHCII from *B. corticulans* at 77 K are quite congested, we show in this paper that the fitting method still converges to a meaningful result. Essential features in the experimental data are well replicated in the fit, giving us more insights into the EET in *B. corticulans* LHCII and demonstrating the strength of this approach to analyze 2DES data of EET processes in general.

2. METHODOLOGY

We applied a phenomenological modeling approach described by Dostál et al.[14] with modifications by Do et al.[11] to simulate the experimental 2DES data of LHCII from *B. corticulans* at 77 K, which were collected in an earlier work.[12] The 2D spectra are all purely absorptive, i.e., they are the sum of the rephasing and nonrephasing signals. A detailed account of the modeling procedure is given in the Supporting Information. Briefly, the model consists of N excitonic energy states with energies E, transition dipole moments μ, spectral widths G, correlation parameters ρ (degree of correlation between each pair of excited and detected states), and two matrices describing the kinetics—the transfer-rate matrix $\mathbf{K}$ and the crosspeak intensities at zero waiting time $\mathbf{X}$. The spectral widths mostly account for static disorder, while the reorganization energy is included in the model as a constant amount of the Stokes shift in all excitonic states. The transfer rate matrix $\mathbf{K}$ describes the population transfer between the excitonic states, where downhill rate constants (from higher- to lower-energy states) are free-fit parameters and uphill rates are inferred from the detailed balance condition for the given temperature.[16] The rate constants are time-independent, and thus the system is assumed to be closer to the Förster regime.[17] The matrix $\mathbf{X}$ describes couplings between excitonic states, which could give rise to crosspeaks at waiting time $T_w = 0$ and partly compensate for the fast EET (<100 fs) that is not experimentally resolved. The 2D electronic spectra were simulated by evaluating the dynamic population transfer between excitonic states at different waiting times T_w, which

https://dx.doi.org/10.1021/acs.jpcb.0c10634
J. Phys. Chem. B 2021, 125, 1134−1143

gives the intensities of various 2D diagonal peaks and crosspeaks with peak shapes defined by the corresponding spectral parameters. A phenomenological excited-state absorption (ESA) spectrum is also included with a single-scaling fit parameter α that controls its intensity. The model parameters were adjusted by nonlinear least-squares optimization to fit the simulated 2D spectra to the experimental data, minimizing the sum of the squared residuals.

3. RESULTS AND DISCUSSION

3.1. Excitonic Energy Levels. A model consisting of eight excitonic states was found to provide a reasonable description of the data, while the majority of kinetic and spectral fit parameters remained independent (see Supplementary Figures S1−S3). Because of the large parameter space, it is challenging to find the global minimum using conventional nonlinear least-squares algorithms, which is why we conducted parallel minimization cycles with randomized starting parameters. Out of 1000 minimization cycles, 80 converged to the same sum of squared residuals (Supplementary Figure S4) and spectral parameters with negligible standard deviations (Table 1), strongly suggesting that a global minimum was found and that the "best-fit" solution is unique. In the following, we will analyze this solution. The discovery of a unique solution for *B. corticulans* LHCII is different from the case of higher-plant LHCII,[11] where the fit resulted in two clusters of possible solutions. Admittedly, in about one-half of all cycles, the sum of the squared residuals was still within 10% of the minimum, but with different combinations of kinetic parameters (Supplementary Figure S5); these other possible solutions will not be regarded further.

The eight excitonic states in the model evidently underrepresent the system, which includes 14 Chls in potentially multiple conformations.[4] The model reproduces the linear absorption spectrum well in the long-wavelength region but deviates at wavelengths shorter than 655 nm (Figure 1). As the excitation spectrum, and consequently the 2D signal, falls sharply, some states absorbing in this wavelength region are not resolved in the model. Additionally, the resolved energy states, especially the "bulk" 650 nm state, may cover multiple near-degenerate excitonic states in the real system.

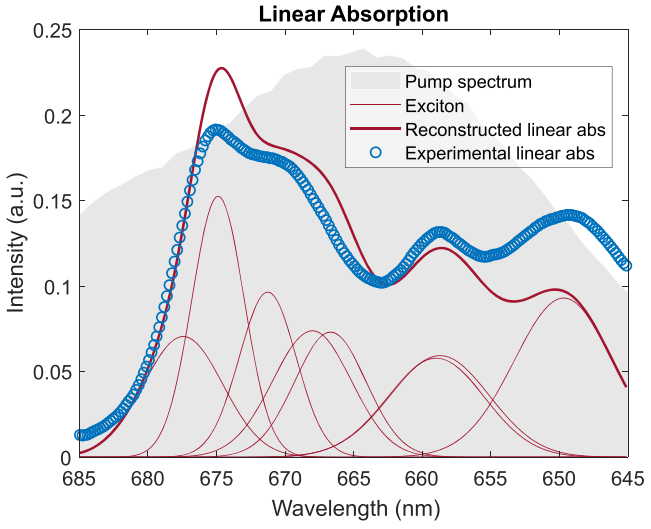

Figure 1. Simulated linear spectra of individual excitonic energy levels and their sum (red curves) calculated from the best fit. The experimental linear absorption (circles) and excitation pump spectrum (shaded area) are also shown.

The replacement of some Chls *a* by Chls *b* in the *B. corticulans* LHCII incurs changes to the excitonic energy levels. Compared to the previous work by Do et al.,[11] which applied a similar fitting procedure to the LHCII from pea, the energy levels resolved from *B. corticulans* are blue-shifted; this finding is in agreement with the analysis of its linear optical spectra.[12] Especially notable are that the 680 nm state is missing in *B. corticulans* and the lowest energy state is centered at 677 nm. Furthermore, the higher number of Chl *b* molecules can result in strongly red-shifted Chl *b* excitonic states due to the higher coupling strengths between them. Therefore, it should be noted that among the resolved states absorbing in the wavelength region typically ascribed to Chls *a* (λ > 660 nm) some could be contributed from red-shifted Chls *b* instead.

The transition dipole moments of all states are of a comparable magnitude except for the "bulk" 650 nm state, which is another indication that it encompasses more than one physical excitonic state. The 675 nm state also has a higher dipole moment in agreement with the strong absorption at around 675 nm in the linear absorption spectrum. The spectral widths (half-width at half-maximum) vary from around 100 to 50−70 cm^{-1} in the high- and low-energy regions, respectively. The bandwidth in the high-energy region is likely overestimated to compensate for the fact that there are fewer resolved states than are physically present. In the long-wavelength region (λ > 660 nm), the difference in the model detail is illustrated in Figure 1, showing the high density of the resolved excitonic bands. As the states in this region are well-resolved, their estimated widths are more reliable.

The antidiagonal widths (half-width at half-maximum) of the diagonal peaks can imply the homogeneous broadening and spectral diffusion of the excitonic states, indicating the tendency of a state to lose its memory of the excitation energy over time.[18] The antidiagonal width can be calculated from the correlation parameters in ρ and the spectral widths in G as

$$H_i = G_i\sqrt{1 - \rho_{ii}}$$

The smaller the antidiagonal width is, the smaller the fluctuations in energies of the pigment molecules are. This may indicate that the binding sites around the Chls in those states are more rigid, leading to smaller nuclear fluctuations in the pigments.[19] We observed that the states at around 659, 671, 675, and 677 nm have smaller homogeneous widths relative to the other states, which yields information about the pigment location and environment.

3.2. Simulated 2D spectra. The simulated and experimental spectra at three key waiting times T_w = 100 fs and 1 and 10 ps are compared in Figure 2. At T_w = 100 fs, the EET has yet to occur, and the signal lies predominantly along the diagonal line; transient crosspeaks due to EET are observed at T_w = 1 ps, and after 10 ps the energy equilibration has largely completed and only the lowest-energy states remain populated. The simulated spectra reproduce the features of the experimental spectra at all three waiting times remarkably well. Some small signals at short wavelengths are more pronounced in the simulated spectra than in the experimental spectra (e.g., the 650 and 659 nm diagonal bands at 100 fs and 1 ps). It is possible that the bleaching signals are masked in the experiment by ESA or simply data noise. These diagonal

https://dx.doi.org/10.1021/acs.jpcb.0c10634
J. Phys. Chem. B 2021, 125, 1134−1143

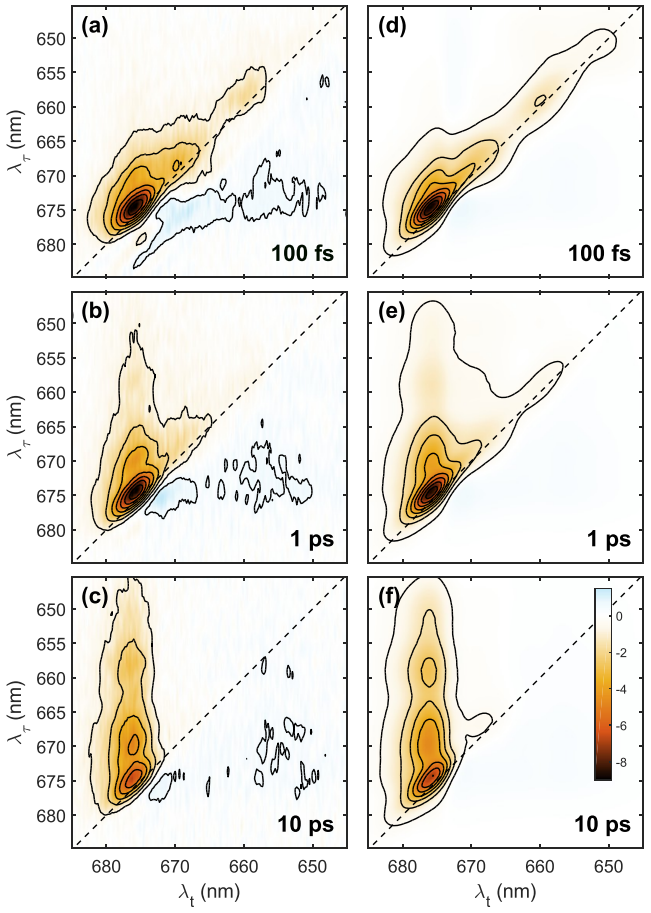

Figure 2. 2D purely absorptive spectra from (a–c) the experimental data and (e–f) the simulated data at T_w = 100 fs (a and d), 1 ps (b and e), and 10 ps (c and f). The vertical axis λ_τ and horizontal axis λ_t represent the wavelengths of the excitation and detection energy, respectively. All spectra use the same color scale. The contour lines are placed at every 12.5% intensity of the highest signal.

features must exist because corresponding crosspeaks are clearly visible at later times (10 ps).

Experimental and simulated kinetic traces at selected excitation/detection wavelengths are compared in Figure 3. The model does not reproduce the amplitude beatings of the diagonal peaks, especially at 671, 675, and 677 nm. As the oscillations are of small amplitudes and disappear quickly, they can be neglected. Apart from that, we can see that at the diagonal peaks and the selected crosspeaks the model fits the experimental dynamics very well. Some deviation at early waiting times (T_w < 0.5 ps) can be observed, especially in the 668 → 676 nm crosspeak, which might suggest that some EET processes are missing in the model. In fact, since the energy levels in the 665–670 nm region are quite congested, it is difficult to recognize all individual dynamic patterns here.

For a more robust inspection of how the model fits the experimental dynamics, we applied a global lifetime analysis of the kinetic traces and compared the model and experimental 2D decay-associated spectra (2D DAS). The 2D DAS obtained from a four-exponential fit (Figure 4) provide an excellent fingerprint for the overall system dynamics, albeit at a reduced level of detail, which can be used as a reference to evaluate the model dynamics.[20] The negative and positive amplitudes in the 2D DAS respectively indicate the decay and rise of the negative signals, i.e., ground-state bleach and simulated emission signals. EET is generally recognized as pairs of oppositely signed peaks along the same excitation wavelengths. The lifetimes and 2D DAS features and amplitudes of the simulated data are in excellent agreement with the experimental data. Some small peaks in the first experimental 2D DAS (Figure 4a) near the diagonal at 675 nm are not present in the simulated 2D DAS. Those signals could be due to coherent artifacts (pulse overlap effects) or quantum-beating signals in this region, which are not represented in the model. Another feature missing from the simulated data is the decay of the crosspeak at 659 → 668 nm in the second 2D DAS (Figure 4b and f). This is in line with the earlier observation that some transfer processes in the 665–670 nm region might be missing from the model. Apart from those, the 2D DAS demonstrate that the detailed excitation dynamics in the complex are well-described by the model.

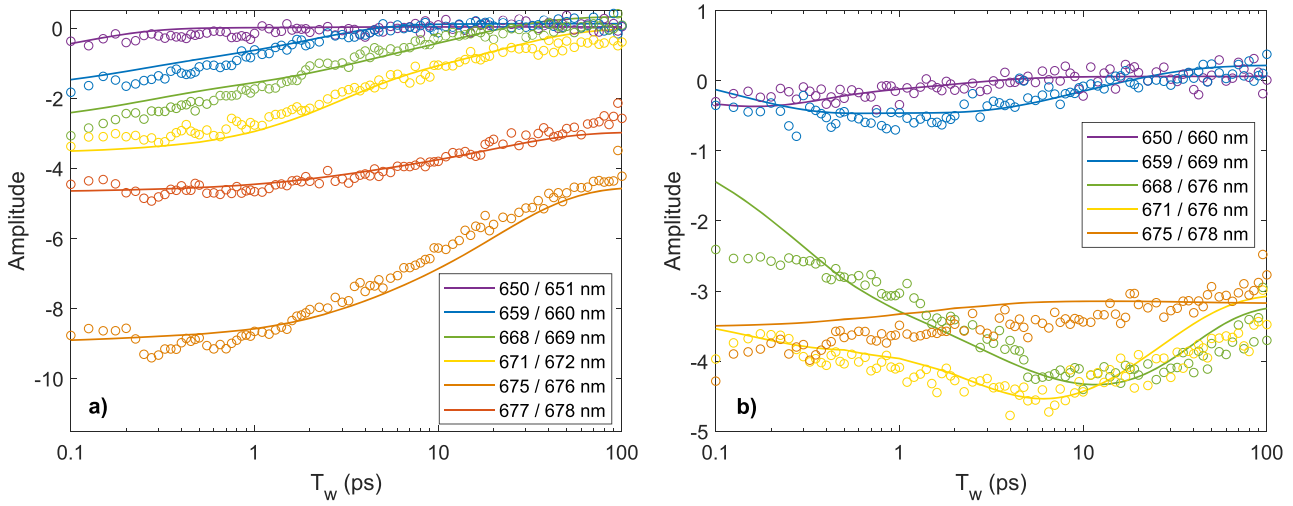

Figure 3. Representative kinetic traces of selected (a) diagonal and (b) off-diagonal signals. The excited/detected wavelengths are denoted in the legends. The detected wavelengths are red-shifted by ∼1 nm with respect to the detected states' absorption wavelengths due to the Stokes shift imposed in the simulation. The results show a good agreement between the experimental data (circles) and the fit (solid curves).

https://dx.doi.org/10.1021/acs.jpcb.0c10634
J. Phys. Chem. B 2021, 125, 1134–1143

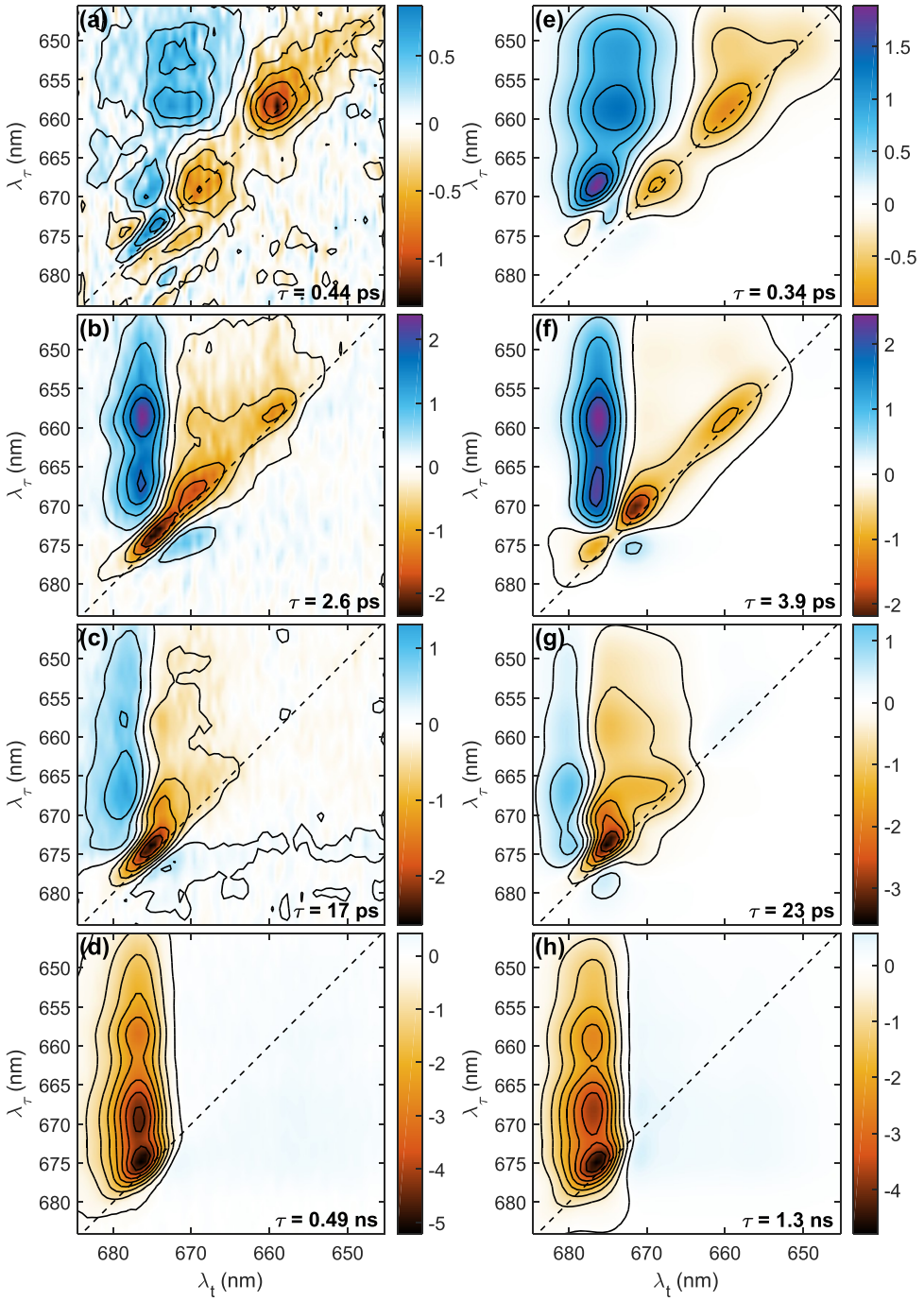

Figure 4. 2D DAS of (a–d) the experimental data and (e–h) the simulated data. The contour lines are drawn as in Figure 2.

3.3. System Dynamics. The specific information about the dynamics of the system is contained in the transfer rate matrix **K** and the crosspeak intensity matrix **X**. Table 2 shows all the significant EET rate constants (≥0.01 ps^{-1}) of the population transfer between states, both downhill and uphill. Green-shaded cells represent high values of the **X** matrix elements, indicating a strong coupling between the corresponding states. The fastest-resolved EET steps are in the Chl *b* domain, particularly from the "bulk" 650 nm state as well as from the 659′ nm state. High rate constants were also found between 668 nm and 671–675 nm. Conversely, the 659 and 667 nm as well as the low-energy Chl *a* states (671, 675, and 677 nm) relax with slower rates (<1 ps^{-1}). On the other hand, the **X** matrix elements indicate a strong coupling between the intermediate and low-energy states—667–671 nm as well as 671–675–677 nm. The coexistence of a strong coupling (crosspeak at T_w = 0) and slow EET generally indicates the presence of more than one excitonic state at the same wavelength. For instance, the 671 nm state probably represents two degenerate states, one weakly coupled and one strongly coupled to lower-energy excitonic states. It is also possible that apparent zero-time crosspeaks between adjacent levels (e.g., 675 → 677 nm) have vibrational origins. With these considerations, we can distinguish two strongly coupled Chl *a* clusters— 667–671 and 671–677 nm—in which fast

https://dx.doi.org/10.1021/acs.jpcb.0c10634
J. Phys. Chem. B 2021, 125, 1134–1143

Table 2. Rate Constants (ps^{-1}) between the Excitonic States[a]

Acceptor \ Donor	650	659	659′	667	668	671	675	677
650		0.07	0.11					
659	3.44							
659′	6.45			0.12	0.06			
667			3.22					
668		0.01	2.67			0.59	0.10	
671		0.30		0.01	2.29		0.02	
675				0.01	1.80	0.09		0.01
677		0.16			0.10		0.04	

[a]Downhill or uphill transfers are in the lower or upper triangle, respectively. Rate constants lower than 0.01 ps^{-1} are omitted. The cells shaded in green indicate the strong coupling between states manifested as high values in **X**.

subpicosecond relaxation occurs but connections between them and the other states are slow.

Figure 5 shows the population of each individual excitonic state over time, which was calculated from the transfer rate matrix in Table 2, and the contribution of that state's population to the observed kinetic lifetimes. The contribution amplitudes were obtained from the matrix **M** inferred from the formula

$$\mathbf{p}(T_w) = \mathbf{M}\exp(\mathbf{L}T_w)$$

where $\mathbf{p}(T_w)$ is the vector of the population at waiting time T_w of the eight excitonic states and **L** is the diagonal matrix, whose elements are the eigenvalues of **K**. The inverse of elements in **L** are thus the kinetic lifetimes of the system. Each column in Figure 5b can be thought of as the contribution of each state in the respective kinetic lifetime. The positive and negative values in the matrix mean the decay and rise, respectively, of the state population.

Population Dynamics of Chls b. The bulk Chl *b* states absorbing at 650 nm funnel the excitation energy to the next two excitonic states at 659 nm and onward to the Chl *a* manifold. It can be seen that lifetimes in the range of 100−170 fs represent downhill transfers from 650 to 659′ nm (100 fs) as well as from 659′ to 667 and 668 nm (170 fs). As a result, the populations of the 650 and 659′ nm states are depleted within 1 ps. For comparison, these fast spectral equilibration features were observed in the first 2D DAS (Figure 4a and e).

The data show the presence of a relatively long-lived Chl *b* state absorbing around 659 nm, which is weakly coupled to the Chl *a* domain. This is evidenced by the slow rates of transfer and a population decay with a lifetime of 1.9 ps. The relaxation of the 659 nm state is also observed in the 2.6 ps experimental 2D DAS (Figure 4b). The fact that the 659 nm and 659′ nm states evolve with significantly different dynamics, although they are not spectrally distinct and cannot be easily spotted by inspecting the 2D spectra alone, is crucial to reconstruct the EET network. On the other hand, the 2D spectra suggest that some population of states around 650 nm decays on an even slower time scale, up to ∼10 ps. Such slowly relaxing Chl *b* states are lacking in the current model, either because of insufficient data fidelity in the Chl *b* region or because they only exist in a fraction of the complexes.

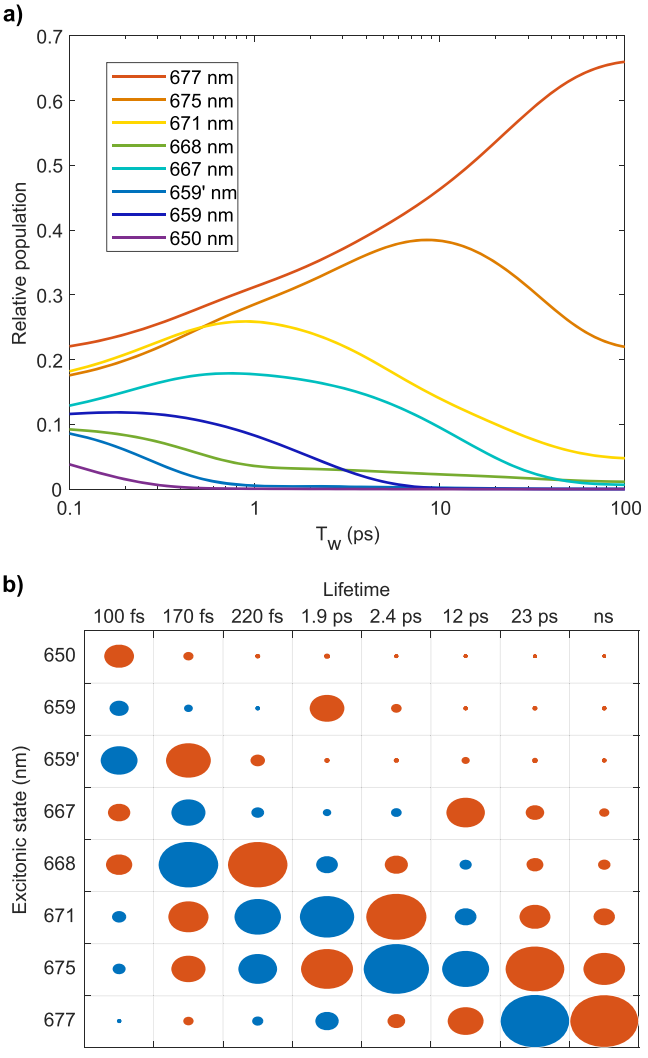

Figure 5. Population kinetics of the eight excitonic states estimated from the model, assuming broadband excitation conditions. (a) Time evolution of the population of each excitonic state. Note the logarithmic time scale. (b) Contributions of the excitonic states to the kinetic lifetimes of the system. The ellipse areas indicate the values of the contribution amplitude matrix **M**. Red or blue ellipses indicate a decaying or rising population, respectively.

Intermediate Energy States. Apart from the long-lived state at 659 nm, the population kinetics (Figure 5a) show states in the intermediate wavelength region at 667 and 671 nm that are rapidly populated but decay at relatively slow rates, suggesting their weak connection to lower energy levels. The former relaxes on a time scale of 12 ps and the latter on a time scale of 2.4 ps (Figure 5b). The earlier analysis by some of us of the 2DES data of LHCII from *B. corticulans* acquired at both room temperature and 77 K also revealed a long-lived state around 669 nm.[12] In plant LHCII, a similar bottleneck state was found to decay on a 4−6 ps time scale at 77 K.[11] Short-lived states also occupy the intermediate wavelength region; the most noticeable is the state at 668 nm, which has subpicosecond transfers to the lower Chl *a* states (220 fs). The short-lived intermediate states are crucial not only for bridging the high-energy Chls *b* and the terminal states but also for connecting the terminal Chl *a* clusters (see below).

Energy Equilibration between Chl a States. Excitonic relaxation within the strongly coupled Chl *a* clusters can occur

https://dx.doi.org/10.1021/acs.jpcb.0c10634
J. Phys. Chem. B 2021, 125, 1134−1143

on very fast time scales (<100 fs), as has been shown for plant LHCII,[21,22] and can also be inferred from the crosspeaks at T_w = 0 (Table 2). Short energy equilibration lifetimes (100−220 fs) are also observed, notably from 668 to 671−675 nm. On the other hand, the Chl *a* clusters are connected to each other via significantly slower EET, as seen by the equilibration lifetimes between the three lowest levels—2.4 ps from 671 to 675 nm and 23 ps from 675 to 677 nm (Figure 5b). Energy equilibration at 77 K is thus complete within around 50 ps, after which the populations of all but the last three states become negligible. The terminal excitonic states decay to the ground state on a nanosecond time scale (the last column in Figure 5b), as illustrated in the final 2D DAS (Figure 4d and h).

The above analysis is summarized in the EET scheme for *B. corticulans* LHCII at 77 K (Figure 6), where the energy levels

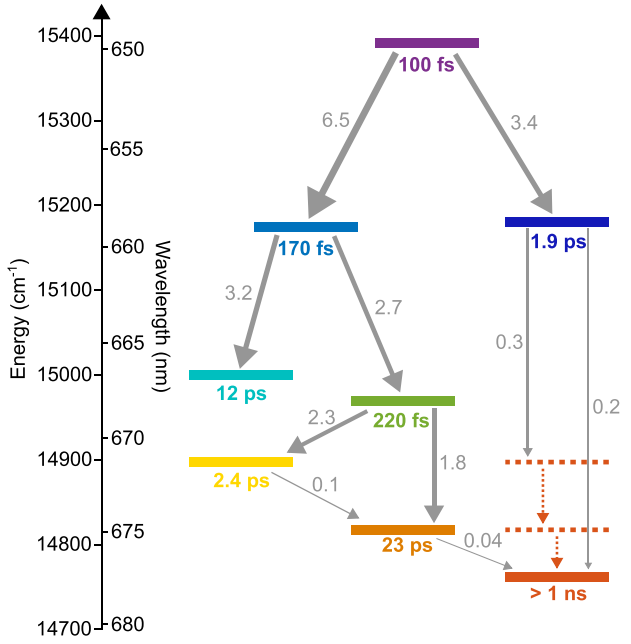

Figure 6. EET scheme for *B. corticulans* LHCII at 77 K. The colored bars represent excitonic energy levels, where dotted lines indicate the excitonic or vibronic levels in the coupled clusters recognized via the **X** matrix. The main kinetic lifetime (energy-transfer time scales) of each state is given below the respective colored bar. Arrows show the major routes of exciton relaxation, with the arrow thickness indicating the EET rate. The rate constants (ps^{-1}) are shown beside the arrows.

are shown along with their respective kinetic lifetimes and transfer rate constants to the other states, according to Table 2 and Figure 5. As mentioned in the System Dynamics section, degenerate excitonic states can appear at some energy levels, which can be seen at 671 and 675 nm in the scheme. The inclusion of these degenerate states helps to explain the slow connections between strongly coupled spectral regions. However, this also results in seven excitonic states in the Chl *a* region, which is one more than what *B. corticulans* LHCII should have.[4] One of these states could have a vibronic origin or be contributed by a strongly red-shifted Chl *b*, as discussed earlier.

The scheme clearly depicts the general flow of energy in *B. corticulans* LHCII at 77 K, where the energy is transferred from high-energy Chls *b* to the intermediate states and then equilibrated among three separate terminal Chl *a* states at 671, 675, and 677 nm. The presence of three weakly connected terminal states also appeared in previous studies of higher-plant LHCII.[7,11,21] In the plant LHCII, the exciton clusters are localized in different locations in the complex, allowing energy flow through multiple pathways and distributing the excitation energy in the equilibrated state. This feature is retained in the LHCII of *B. corticulans*, as can be expected from the structural similarity of the complexes. It is also worth pointing out that the equilibration lifetimes between the terminal states are determined mainly by the uphill transfer to higher excitonic levels (the dominating rate constants in Table 2) rather than by the direct transfer between the sink states. The same behavior was found in higher-plant LHCII.[11] Apart from these basic common features for both types of LHCII, there are significant quantitative differences between them. A direct comparison with a similar phenomenological model of higher-plant LHCII[11] shows slower EET steps among Chl groups in *B. corticulans*. For instance, the long-lived state around 665−668 nm has a 2−6 ps decay lifetime in plant LHCII versus a 12 ps decay lifetime in *B. corticulans*; the EET between states at 671−675 nm can be up to several-fold slower. The specific differences corroborate the finding of an overall slower EET from Chl *b* to *a* and within the Chl *a* domain based on 2D DAS.[12]

In summary, modeling the experimental data with eight excitonic states, which yields the above-described kinetics, offers a significantly greater potential to describe the system dynamics than a global lifetime analysis (2D DAS) even though not all model fit parameters can be regarded as completely independent. With the acquired fitting parameters, necessary information about the system has already been obtained, and a transfer scheme can be constructed for the EET network in *B. corticulans* LHCII. The scheme at this state can provide the connections between the energy levels and can be used to deduce some insights about the structure of the complex, i.e., the constituent Chl pigments on which the various excitons are localized. Thus, an attempt to interpret the structural information of the complex based on the fit results is presented in the next section.

3.4. Pigment Replacement Calculation and Structure Predicting Attempt. Exciton modeling based on the existing Hamiltonian of the plant LHCII complex was conducted to check whether the excitonic energy levels in *B. corticulans* LHCII from the model could be reproduced in plant LHCII with two Chls *a* replaced by Chls *b*.[23] An assumption was made in this calculation that the complex structure in *B. corticulans* LHCII is similar to that in plants. Hence, the calculation was performed by taking the structural model for the plant LHCII trimer and changing the transition site energies and dipole moments of two Chls *a* in every monomer into those of Chls *b*.[5] Two different Hamiltonians of plant LHCII were considered in this pigment-replacement calculation. One was obtained from the *ab initio* quantum calculation of Müh et al.,[23] and the other one was retrieved from the modified Redfield-generalized Förster model of Novoderezhkin et al.[24] The site energies and transition dipole moments were modified by the average difference between the Chl *b* and Chl *a* states in the original plant Hamiltonian for each Chl *a* → *b* replacement. In all cases, the transition dipole was centered at the magnesium atom and aligned along the vector connecting the nitrogen atoms NB and ND (the conventional *y*-axis of the chlorin ring) in the structure file. We thus assume that the effect of the protein environment is the

https://dx.doi.org/10.1021/acs.jpcb.0c10634
J. Phys. Chem. B 2021, 125, 1134−1143

same in the algal and plant complexes. Since there are eight Chls *a* in a monomer, it gives us a total of 28 possible replacement combinations for each Hamiltonian. The excitonic energy levels of each combination were extracted by diagonalizing the corresponding Hamiltonian and were then compared with this work by taking the sum of the squared differences between those diagonalized energy levels and their nearest levels in Table 1.

The replacement combinations were first evaluated by comparing the lowest energy level, which should be blue-shifted in *B. corticulans* LHCII compared to that in plant LHCII. Such blue-shifting appears in the calculated excitonic energy levels of the alternate structures when at least one pigment in the Chl *a*610−611−612 trimer is replaced by Chl *b* (Figure 7). This is predictable as this Chl *a* trimer has been well-assigned as the main contributor to the lowest-energy sink in plant LHCII.[22,24] However, only a few of those alternate structures result in a similar set of excitonic levels to the phenomenological fit, which should be indicated by a low sum of the squared differences. As a result, using the Hamiltonian from Müh et al.[23] suggests that a pigment replacement in the Chl *a*604 and *a*610 pair is the most probable choice (Figure 7a). It is also interesting to note that the same Chls were identified as likely candidates for the *a*/*b* exchange based on the anisotropic circular dichroism spectra of LHCII from *B. corticulans*.[12,25] On the other hand, the Hamiltonian from Novoderezhkin et al.[24] suggests the replacement of Chl *a*602 and either Chl *a*612 or *a*611 (Figure 7b), while the replacement of Chl *a*610 in this case is not probable since it does not cause a spectral blue shift (Supplementary Figure S8). Thus, it can be seen that the predictions of pigment identities vary with the Hamiltonian used. This may be due to either the differences between the ways these Hamiltonians are constructed[26] or substantial differences between the *B. corticulans* and plant LHCII structures.

Despite the limitations described, attempts to construct the EET scheme based on the suggested pigment identities as an exercise of curiosity were conducted and are provided in the Supporting Information along with a discussion. However, as much as the discussion is made for those proposed EET schemes, they can only hold with the initial assumptions that the crystal structure of *B. corticulans* LHCII is similar to the plant LHCII. Hence, while the proposed schemes do not serve as predictions for the spatial network of EET in *B. corticulans* LHCII they can be used as references for future studies about the system as well as the higher-plant counterpart. Additionally, the fact that the use of different Hamiltonians results in different EET schemes indicates the importance of finding a robust method to describe the LHCII system, and the *B. corticulans* LHCII can be a test to verify the reliability of those Hamiltonians.

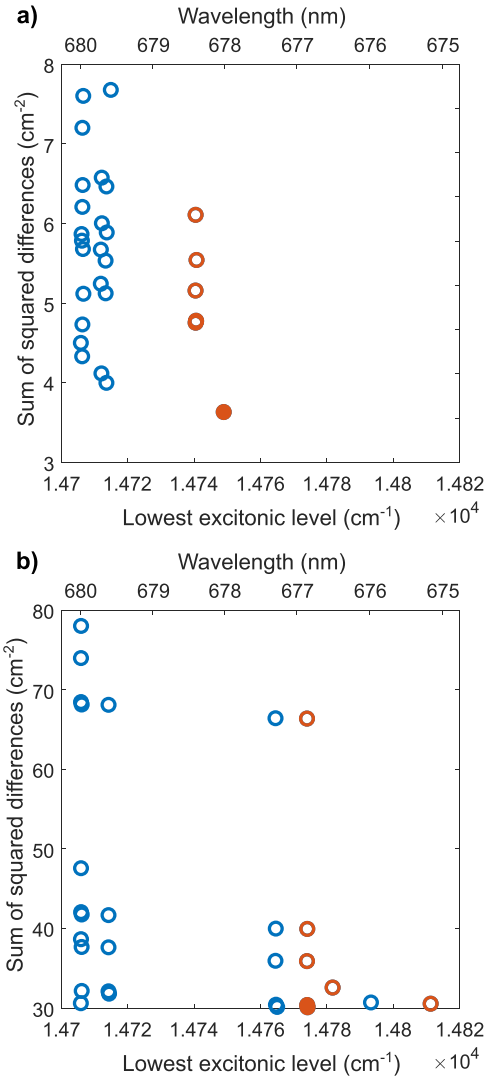

Figure 7. Scatter plots of the sum of the squared differences between the phenomenologically fitted excitonic levels and those from each of the 28 combinations where two Chl *a* were replaced by Chl *b* molecules. The horizontal axis shows the lowest energy level of the combinations. The original plant LHCII Hamiltonians were obtained from (a) Müh et al.[23] and (b) Novoderezhkin et al.[24] In panel a, the combinations involving the replacement of site 610 are red-colored. The filled data point indicates the combination with replacements in sites 604 and 610. In panel b, the combinations involving the replacement of site 612 are red-colored. The filled data point indicates the combination with replacements in sites 602 and 612. The plot involving the replacement of site 611 is similar and is shown in Supplementary Figure S8.

4. CONCLUSIONS

The light-harvesting system of *B. corticulans* is adapted for the enhanced absorption of short-wavelength, especially blue-green, light when the alga is submerged underwater. The enrichment of Chl *b* in LHCII contributes to the absorption of shorter-wavelength red light and blue-green light. It could be expected that Chl *b* also facilitates an energetic coupling with the carotenoids siphonein and siphonoxanthin through the better spectral overlap of the Soret and the carotenoid S_2 transitions, although experimental evidence suggests that these carotenoids transfer energy to Chl *a* only.[9] The adaptive pigment composition change has a consequence on the dynamics of EET in the complex. The information obtained from the phenomenological modeling of the 2DES data at 77 K aligns with the previous 2DES analysis while providing significant detail, particularly about the properties and dynamics of excitonic states in the Chl *a* domain. As can be expected for structurally homologous complexes, the excitonic states and EET dynamics closely resemble those of higher-plant LHCII. After excitation, energy is transferred from Chls *b* to Chls *a* on subpicosecond time scales, with slower EET components particularly from a state absorbing at 659 nm. The Chl *a* region consists of three exciton clusters with lower-energy states at 671, 675, and 677 nm. Thus, the *B. corticulans*

https://dx.doi.org/10.1021/acs.jpcb.0c10634
J. Phys. Chem. B 2021, 125, 1134−1143

complex loses the lowest-energy exciton state (around 680 nm), which in plant LHCII supposedly plays a significant role in mediating excitation migration to PSII. Apart from the rapid relaxation components within the domains, the equilibration between them occurs on time scales up to about 20 ps. Uphill energy transfer to higher-energy excitonic states is crucial to bridge the terminal sinks. The lower density of the Chl *a* excitonic states (or chromophores in a space domain) results in an overall slower exciton equilibration compared to that of plant LHCII, which can be seen in the longer relaxation times of the 668, 671, and 675 nm exciton states. There appears to be a trade-off between the spectral adaptation and the optimal EET. Interestingly, the minor loss of a light-harvesting function that could be expected from a slower EET is compensated by a longer excitation lifetime in the *B. corticulans* LHCII.[13] At any rate, the enhanced capacity of the algal light-harvesting antenna for photoprotection via sustained nonphotochemical quenching[27] and the effective quenching of the Chl triplet states[13] is probably more significant from a physiological and evolutionary standpoint.

The phenomenological model allows us to construct a quantitative scheme for the EET in LHCII of *B. corticulans* at 77 K, visualizing the energy-transfer pathways between energy levels that are represented by spectral components in the complex. An attempt to assign the sites that likely bind Chls *b* in *B. corticulans* instead of Chls *a* as in higher plants was conducted, but the results were not conclusive. It will be of interest to compare detailed structure-based calculations (when they become available) with the predictions made by the phenomenological fitting. Nevertheless, the robustness of the phenomenological approach to extract valuable molecular information from the 2DES data has been put to a good test with the *B. corticulans* LHCII system. With further improvements in the future, the method promises to be a useful analysis tool for 2DES data of complex energy-transfer systems.

■ ASSOCIATED CONTENT

Supporting Information

The Supporting Information is available free of charge at https://pubs.acs.org/doi/10.1021/acs.jpcb.0c10634.

The phenomenological fitting procedure; fitting results with six, seven, and nine states; best-fits of the eight-state fitting; calculation of the ESA spectrum; effects of the correlation parameter on the 2D peak shape; and discussion on the pigment replacement calculation (PDF)

■ AUTHOR INFORMATION

Corresponding Authors

Howe-Siang Tan − *Division of Chemistry and Biological Chemistry, School of Physical and Mathematical Sciences, Nanyang Technological University, Singapore 637371;* orcid.org/0000-0003-2523-106X; Email: howesiang@ntu.edu.sg

Petar H. Lambrev − *Biological Research Center, Szeged, Szeged 6726, Hungary*; Email: lambrev.petar@brc.hu

Authors

Hoang Long Nguyen − *Division of Chemistry and Biological Chemistry, School of Physical and Mathematical Sciences, Nanyang Technological University, Singapore 637371; University of Groningen, Zernike Institute for Advanced Materials, 9747 AG Groningen, The Netherlands*

Thanh Nhut Do − *Division of Chemistry and Biological Chemistry, School of Physical and Mathematical Sciences, Nanyang Technological University, Singapore 637371*

Parveen Akhtar − *Biological Research Center, Szeged, Szeged 6726, Hungary; ELI-ALPS, ELI-HU Nonprofit Ltd., Szeged 6728, Hungary*

Thomas L.C. Jansen − *University of Groningen, Zernike Institute for Advanced Materials, 9747 AG Groningen, The Netherlands;* orcid.org/0000-0001-6066-6080

Jasper Knoester − *University of Groningen, Zernike Institute for Advanced Materials, 9747 AG Groningen, The Netherlands*

Wenda Wang − *Photosynthesis Research Center, Key Laboratory of Photobiology, Institute of Botany, Chinese Academy of Sciences, 100093 Beijing, China*

Jian-Ren Shen − *Photosynthesis Research Center, Key Laboratory of Photobiology, Institute of Botany, Chinese Academy of Sciences, 100093 Beijing, China; Research Institute for Interdisciplinary Science, Graduate School of Natural Science and Technology, Okayama University, Okayama 700-8350, Japan;* orcid.org/0000-0003-4471-8797

Complete contact information is available at: https://pubs.acs.org/10.1021/acs.jpcb.0c10634

Notes

The authors declare no competing financial interest.

■ ACKNOWLEDGMENTS

H.-S.T acknowledges support from the Singapore Ministry of Education Academic Research Fund (Tier 1 RG2/19 and Tier 1 RG15/18). P.H.L. acknowledges grants from the National Research, Development and Innovation Fund (Grants NN-124904 and 2018-1.2.1-NKP-2018-00009). This work was also supported by a Strategic Priority Research Program (XDB17030100) of China, a Key Research Project for Frontier Science (QYZDY-SSW-SMC003) from the Chinese Academy of Sciences (CAS), China, and a bilateral project between CAS and the Hungary Academy of Sciences.

■ REFERENCES

(1) Blankenship, R. E. *Molecular Mechanisms of Photosynthesis*, 2nd ed.; Wiley, 2014.

(2) Mirkovic, T.; Ostroumov, E. E.; Anna, J. M.; van Grondelle, R.; Govindjee; Scholes, G. D. Light Absorption and Energy Transfer in the Antenna Complexes of Photosynthetic Organisms. *Chem. Rev.* **2017**, *117*, 249−293.

(3) Kirk, J. T. O. *Light and Photosynthesis in Aquatic Ecosystems*, 2nd ed.; Cambridge University Press, 1994.

(4) Wang, W.; Qin, X.; Sang, M.; Chen, D.; Wang, K.; Lin, R.; Lu, C.; Shen, J. R.; Kuang, T. Spectral and functional studies on siphonaxanthin-type light-harvesting complex of photosystem II from Bryopsis corticulans. *Photosynth. Res.* **2013**, *117*, 267−279.

(5) Liu, Z.; Yan, H.; Wang, K.; Kuang, T.; Zhang, J.; Gui, L.; An, X.; Chang, W. Crystal structure of spinach major light-harvesting complex at 2.72 Å resolution. *Nature* **2004**, *428*, 287−292.

(6) Standfuss, J.; Terwisscha van Scheltinga, A. C.; Lamborghini, M.; Kuhlbrandt, W. Mechanisms of photoprotection and nonphotochemical quenching in pea light-harvesting complex at 2.5 A resolution. *EMBO J.* **2005**, *24*, 919−928.

(7) Renger, T. Theory of excitation energy transfer: from structure to function. *Photosynth. Res.* **2009**, *102*, 471−485.

(8) van Grondelle, R.; Novoderezhkin, V. I. Energy transfer in photosynthesis: experimental insights and quantitative models. *Phys. Chem. Chem. Phys.* **2006**, *8*, 793−807.
(9) Nakayama, K.; Mimuro, M.; Nishimura, Y.; Yamazaki, I.; Okada, M. Kinetic analysis of energy transfer processes in LHC II isolated from the siphonous green alga, Bryopsis maxima with use of picosecond fluorescence spectroscopy. *Biochim. Biophys. Acta, Bioenerg.* **1994**, *1188*, 117−124.
(10) Akhtar, P.; Do, T. N.; Nowakowski, P. J.; Huerta-Viga, A.; Khyasudeen, M. F.; Lambrev, P. H.; Tan, H. S. Temperature Dependence of the Energy Transfer in LHCII Studied by Two-Dimensional Electronic Spectroscopy. *J. Phys. Chem. B* **2019**, *123*, 6765−6775.
(11) Do, T. N.; Huerta-Viga, A.; Akhtar, P.; Nguyen, H. L.; Nowakowski, P. J.; Khyasudeen, M. F.; Lambrev, P. H.; Tan, H. S. Revealing the excitation energy transfer network of Light-Harvesting Complex II by a phenomenological analysis of two-dimensional electronic spectra at 77 K. *J. Chem. Phys.* **2019**, *151*, 205101.
(12) Akhtar, P.; Nowakowski, P. J.; Wang, W.; Do, T. N.; Zhao, S.; Siligardi, G.; Garab, G.; Shen, J. R.; Tan, H. S.; Lambrev, P. H. Spectral tuning of light-harvesting complex II in the siphonous alga Bryopsis corticulans and its effect on energy transfer dynamics. *Biochim. Biophys. Acta, Bioenerg.* **2020**, *1861*, 148191.
(13) Li, D. H.; Wang, W.; Zhou, C.; Zhang, Y.; Wang, P.; Shen, J. R.; Kuang, T.; Zhang, J. P. Excitation dynamics and relaxation in the major antenna of a marine green alga Bryopsis corticulans. *Biochim. Biophys. Acta, Bioenerg.* **2020**, *1861*, 148186.
(14) Dostál, J.; Benesova, B.; Brixner, T. Two-dimensional electronic spectroscopy can fully characterize the population transfer in molecular systems. *J. Chem. Phys.* **2016**, *145*, 124312.
(15) Thyrhaug, E.; Zidek, K.; Dostál, J.; Bina, D.; Zigmantas, D. Exciton Structure and Energy Transfer in the Fenna-Matthews-Olson Complex. *J. Phys. Chem. Lett.* **2016**, *7*, 1653−1660.
(16) Pollard, W. T.; Friesner, R. A. Solution of the Redfield equation for the dissipative quantum dynamics of multilevel systems. *J. Chem. Phys.* **1994**, *100*, 5054−5065.
(17) Kramer, T.; Noack, M.; Reimers, J. R.; Reinefeld, A.; Rodríguez, M.; Yin, S. Energy flow in the Photosystem I supercomplex: Comparison of approximative theories with DM-HEOM. *Chem. Phys.* **2018**, *515*, 262−271.
(18) Hamm, P.; Zanni, M. T. *Concepts and Methods of 2D Infrared Spectroscopy*; Cambridge University Press, 2011.
(19) Thallmair, S.; Vainikka, P. A.; Marrink, S. J. Lipid Fingerprints and Cofactor Dynamics of Light-Harvesting Complex II in Different Membranes. *Biophys. J.* **2019**, *116*, 1446−1455.
(20) Slavov, C.; Hartmann, H.; Wachtveitl, J. Implementation and evaluation of data analysis strategies for time-resolved optical spectroscopy. *Anal. Chem.* **2015**, *87*, 2328−2336.
(21) Novoderezhkin, V. I.; Palacios, M. A.; van Amerongen, H.; van Grondelle, R. Excitation Dynamics in the LHCII Complex of Higher Plants: Modeling Based on the 2.72 Å Crystal Structure. *J. Phys. Chem. B* **2005**, *109*, 10493−10504.
(22) Renger, T.; Madjet, M. E.; Knorr, A.; Müh, F. How the molecular structure determines the flow of excitation energy in plant light-harvesting complex II. *J. Plant Physiol.* **2011**, *168*, 1497−1509.
(23) Müh, F.; Madjet, M. E.-A.; Renger, T. Structure-Based Identification of Energy Sinks in Plant Light-Harvesting Complex II. *J. Phys. Chem. B* **2010**, *114*, 13517−13535.
(24) Novoderezhkin, V.; Marin, A.; van Grondelle, R. Intra- and inter-monomeric transfers in the light harvesting LHCII complex: the Redfield-Forster picture. *Phys. Chem. Chem. Phys.* **2011**, *13*, 17093−17103.
(25) Akhtar, P.; Lindorfer, D.; Lingvay, M.; Pawlak, K.; Zsiros, O.; Siligardi, G.; Javorfi, T.; Dorogi, M.; Ughy, B.; Garab, G.; et al. Anisotropic Circular Dichroism of Light-Harvesting Complex II in Oriented Lipid Bilayers: Theory Meets Experiment. *J. Phys. Chem. B* **2019**, *123*, 1090−1098.
(26) Kreisbeck, C.; Kramer, T.; Aspuru-Guzik, A. Scalable High-Performance Algorithm for the Simulation of Exciton Dynamics. Application to the Light-Harvesting Complex II in the Presence of Resonant Vibrational Modes. *J. Chem. Theory Comput.* **2014**, *10*, 4045−4054.
(27) Giovagnetti, V.; Han, G.; Ware, M. A.; Ungerer, P.; Qin, X.; Wang, W. D.; Kuang, T.; Shen, J. R.; Ruban, A. V. A siphonous morphology affects light-harvesting modulation in the intertidal green macroalga Bryopsis corticulans (Ulvophyceae). *Planta* **2018**, *247*, 1293−1306.

https://dx.doi.org/10.1021/acs.jpcb.0c10634
J. Phys. Chem. B 2021, 125, 1134−1143